

## Article

# Study on the Controlling Factors of Li-Bearing Pegmatite Intrusions for Mineral Exploration, Uljin, South Korea

Il-Hwan Oh <sup>1</sup>, Seok-Jun Yang <sup>1,\*</sup>, Chul-Ho Heo <sup>1</sup>, Jae-Ho Lee <sup>1</sup>, Eui-Jun Kim <sup>1</sup> and Seong-Jun Cho <sup>2</sup>

<sup>1</sup> Critical Minerals Research Center, Korea Institute of Geoscience and Mineral Resources, Daejeon 34132, Korea; ilhwan@kigam.re.kr (I.-H.O.); chheo@kigam.re.kr (C.-H.H.); jhlee@kigam.re.kr (J.-H.L.); euijun.kim@kigam.re.kr (E.-J.K.)

<sup>2</sup> Mineral Resources Division, Korea Institute of Geoscience and Mineral Resources, Daejeon 34132, Korea; mac@kigam.re.kr

\* Correspondence: ysj@kigam.re.kr; Tel.: +82-42-868-3100

**Abstract:** Recently, the demand for lithium (Li) as an energy storage element has increased, owing to the rapid increase in the number of electric vehicles. To meet this demand, Li exploration has become increasingly important. The Boam deposit is located in the Uljin area of eastern South Korea, where several rare-element pegmatites (0.24% Li) intrude the Precambrian Janggun Limestone Formation. In this study, we performed petrographical and geometrical analyses of the rare-element pegmatites recognized in the vicinity of the Boam deposit, through which the Li-mineralization process was identified and the factors controlling intrusion studied. Our results are summarized as follows: (1) the pegmatites exhibit regional and internal zoning based on their mineral assemblages; (2) Li mineralization is restricted to pegmatites; (3) the geometry and distribution of the pegmatites are strongly controlled by fracture, bed contact, and post-intrusive deformation; and (4) exploration should be concentrated in the ENE–WSW-trending zone of the upper part of the Janggun Limestone Formation. These results provide valuable understanding to guide the development of strategies for early-stage mineral exploration in the Uljin area.

**Keywords:** Boam deposit; rare-element pegmatite; Li exploration; geometrical analysis; petrographical analysis



**Citation:** Oh, I.-H.; Yang, S.-J.; Heo, C.-H.; Lee, J.-H.; Kim, E.-J.; Cho, S.-J. Study on the Controlling Factors of Li-Bearing Pegmatite Intrusions for Mineral Exploration, Uljin, South Korea. *Minerals* **2022**, *12*, 589. <https://doi.org/10.3390/min12050589>

Academic Editor: Harald G. Dill

Received: 10 April 2022

Accepted: 5 May 2022

Published: 6 May 2022

**Publisher's Note:** MDPI stays neutral with regard to jurisdictional claims in published maps and institutional affiliations.



**Copyright:** © 2022 by the authors. Licensee MDPI, Basel, Switzerland. This article is an open access article distributed under the terms and conditions of the Creative Commons Attribution (CC BY) license (<https://creativecommons.org/licenses/by/4.0/>).

## 1. Introduction

The high demand for secondary batteries that can be used semi-permanently via charging contributes to the increasing importance of Lithium (Li) as a strategic element [1]. Lithium prices are steadily rising with demand, having increased by more than 200% in 2021 compared with the previous year [2]. To secure Li resources, global producers such as Albemarle (USA), Jiangxi Ganfeng Lithium (China), Pilbara Minerals (Australia), and Sociedad Química y Minera (Chile) are actively investing in Li exploration projects in their respective countries [3]. In South Korea, Li exploration has been conducted in the Uljin area by the Korea Institute of Geoscience and Mineral Resources (KIGAM) since 2013 [4,5].

Lithium is mainly extracted from two sources—brines and hard rocks (i.e., pegmatite, granite, and sedimentary rocks) [3,6,7]. Brine-type deposits are the predominant source (60–70% of global Li supply) and comprise the largest reserves (low-grade), have a low recovery rate, and are less environmentally friendly compared to hard-rock deposits. Hard-rock deposits are typically of higher grade and are easier to mine than brine-type deposits, and often include combinations of high-grade rare elements including Be, Nb, Ta, Rb, and Cs [7–12]. Lithium hosted in hard rock is mainly related to rare-element pegmatite; currently, 26% of the global Li supply comes from these deposits. The estimated total global Li resources in rare-element pegmatite deposits are approximately 3.9 Mt, comprising 24.2% in Australia, 12.4% in China, 30.7% in North America (USA and Canada), 26.8% in South Africa (DRC, Zimbabwe, and Namibia), and 5.4% in Russia [13].

In South Korea, Li mineralization has been reported in the Uljin and Danyang pegmatites and Haenam volcanic rocks [4,5,14–18]. Mining activities took place in the Uljin area, including the Boam deposit, between 1945 and 1963, and yielded approximately 180 Mt of Li orebodies ( $\text{LiO}_2 = 1.69\text{--}1.9\%$ ) [17]. Currently, all Li mining has ceased; however, Li-exploration activities for the evaluation of potential resources are now being undertaken in the Uljin area owing to the increased demand. The Uljin pegmatite intrudes Precambrian gneiss and metasedimentary or sedimentary rocks. The pegmatite bodies have a dyke-sill shape, vary from a few meters to tens of meters in length, and reach several meters thick. Notably, the Li-bearing pegmatites around the Boam deposit have experienced hydrothermal alteration and late deformation; therefore, the evolution and intrusion trends of this deposit are challenging to predict. Previous studies of the Boam Li-bearing pegmatites have generated a range of geochemical, isotopic, and geochronological data [4,5,18]. Lee et al. [5] classified Li-bearing pegmatites into three groups based on their locations (i.e., western, main, and eastern orebodies). The estimated average Li content of each orebody is 1854 ppm, 3566 ppm, and 4474 ppm, respectively. However, they have not considered the geometry and distribution of Li-pegmatite in mineral exploration.

Traditionally, pegmatite exploration techniques can be divided into grassroots and advanced exploration [19]. The goal of grassroots exploration is to find a pegmatite dyke and map its area to evaluate its mineralization potential, while advanced exploration aims to study a pegmatite dyke in more detail, such as the specific location of a mineralization zone [19]. An important commonality between these two research methods is the exploration of pegmatites as a source of economic commodities, relying entirely on surface discoveries [19]. Here, we sought to identify areas of hidden Li orebodies with a high potential for exploitation based on the petrographical and geometrical analysis of exposed thirteen rare-element pegmatites (hereafter referred to as REP). Our results show that the intrusion patterns and distribution characteristics in this area are strongly controlled by fracture, bed contact, and post-intrusive deformation. Overall, our findings provide a valuable understanding of the pegmatite intrusion mechanisms in the study region and may be useful in early-stage exploration.

## 2. Geological Background

The Precambrian basement in the southern part of the Korean Peninsula consists of the Gyeonggi and Yeongnam Massifs. The Yeongnam Massif is located between the Okcheon metamorphic belt and the Taebaeksan Basin in the north and the Gyeongsang Basin in the south (Figure 1a). The Yeongnam massif has experienced tectonic events related to the Early Proterozoic continental collision, with NS- and NE-strike structures [20,21].

The geology of the Uljin area, northeast of the Yeongnam Massif, mainly consists of Precambrian gneiss (Wonnam Formation, Buncheon granite gneiss), metasedimentary (Dongsugok Formation, Yulri Series), limestone–marble (Janggung Limestone Formation), and later intrusions of unknown age (Figure 1a). Pegmatites intrude the Wonnam (Wonnam Formation, Dongsugok Formation, and Janggung Limestone Formation) and the Yulri Series, and are concentrated at the southern NE–SW-trending Buncheon granite gneiss ( $1990 \pm 5$  to  $1813 \pm 377$  Ma) [22,23]. Pegmatite swarms strike  $N30^\circ\text{--}80^\circ$  E, dip  $30^\circ\text{--}80^\circ$  NW, and are divided into two types according to their mineral composition and emplacement age in Uljin. Simple pegmatites are composed primarily of quartz, feldspar, and muscovite, lack internal zoning, and have emplacement ages between  $778 \pm 14$  and  $696 \pm 15$  Ma [15]. REPs are primarily composed of quartz, feldspar, muscovite, and rare-element minerals such as lepidolite, spodumene, elbaite, beryl, cassiterite, fluorite, topaz, and apatite. The REPs were emplaced between  $186 \pm 4$  and  $155 \pm 3$  Ma [15,18,24] and partially experienced hydrothermal alteration (internal greisen). During this period (ca. 200–160 Ma), subduction-related magmatism and the development of a shear zone occurred on the Yeongnam Massif [20].

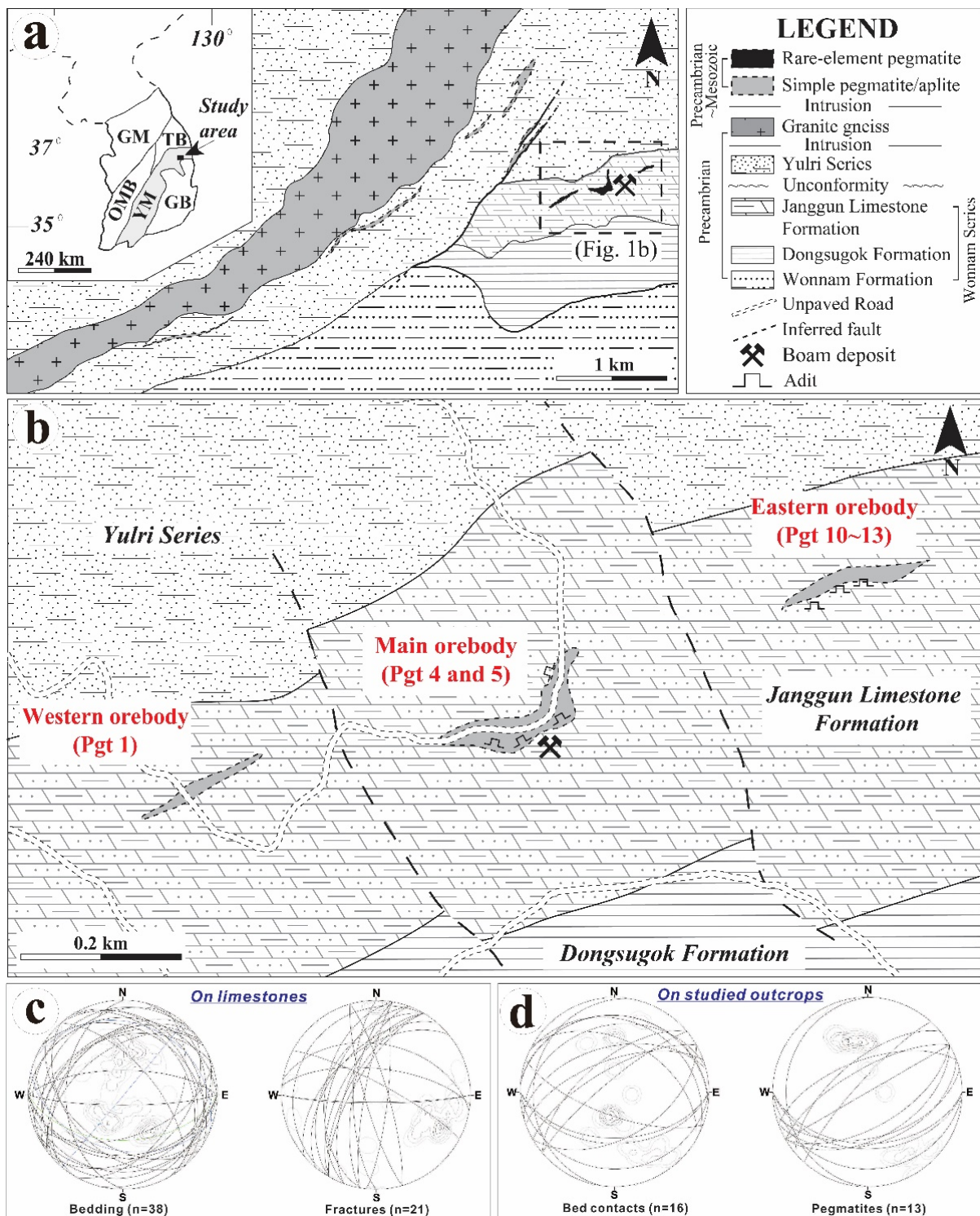


**Figure 1.** (a) Simplified tectonic map of the southern Korean Peninsula and geological map of Uljin, South Korea (modified from [15]). (b) Geological map of the Boam deposit showing the location of the studied pegmatites (modified from [5]). (c) The stereo-nets (equal area, lower hemisphere) show dominant directions of bedding and fractures in Janggum Limestone Formation. (d) The stereo-nets (equal area, lower hemisphere) show dominant directions of bedding and pegmatites in the studied outcrops.

The geology of the Boam deposit, located east of the Uljin area, mainly consists of the Dongsugok Formation, the Janggum Limestone Formation, and the Yulri Series

(Figure 1b). The Dongsugok Formation forms the lowest strata, composed primarily of mica schist and intercalated quartzite-amphibole schist [15]. The Janggung Limestone Formation conformably overlies the Dongsugok Formation. In the lower part of the Janggung Limestone Formation, gray-white to light-pink limestone predominates, whereas light-gray limestone alternates with dark-gray to black sandy limestone in the upper part [15]. The light-gray limestone mainly consists of coarse calcite with minor muscovite, and the dark-gray to black sandy limestone mainly consists of calcite, quartz, tourmaline, and biotite. The upper part of Janggung Limestone Formation often exhibits a nodular texture characterized by centimeter- to tens-of-centimeter-sized nodules floating within a fine-grained sandy limestone matrix.

The dominant directions of the bedding and fractures in the Janggung limestones in the study area are E–W- and NE–SW-striking, respectively (Figure 1b). Most of the bedding shows a low or moderate angle ( $<40^\circ$ ), and frequently changing dip directions are identified from the stereo-net. Although these structures may be related to folding events, more detailed analysis and data are needed to aid interpretation. Most of the fractures show moderate or high angles ( $>50^\circ$ ) and can be grouped into two NE–SW- and E–W-striking sets; however current field data are insufficient to investigate the fracture deformation history, requiring detailed structural work to aid further exploration.

The Yulri Series unconformably overlies the Janggung Limestone Formation and primarily consists of schist, phyllite, quartzite, and partially intercalated limestone. The intercalated limestone layers range from 30 to 100 m in thickness and contain calcite with minor quartz, muscovite, pyrite, and magnetite [15]. The general strike and dip of the Dongsugok Formation, the Janggung Limestone Formation, and the Yulri Series are  $N30^\circ\text{--}80^\circ\text{ E}$  and  $30^\circ\text{--}80^\circ\text{ NW}$ , respectively, but include complex structures due to local folding and faulting.

### 3. Research Methods

#### 3.1. Geochemical and Petrographical Analysis

Seven fresh REP samples were collected from orebodies during geological mapping for analysis, and polished thin-sections were prepared for petrographic study. Samples BA1–3 are representative REP samples selected from each orebody for comparison with existing data, while samples BAN1–4 are REPs newly identified as part of this study (Table 1). Rare-element analysis was conducted by inductively coupled plasma mass spectrometry (ICP-MS) and inductively coupled plasma optical emission spectrometry (ICP-OES) at Activation Laboratories Ltd., Ontario, Canada, and the Korea Institute of Geoscience and Mineral Resources (KIGAM), Daejeon, Korea. The powdered rock samples (approximately 0.5 g) were dissolved in an acid mixture at  $190^\circ\text{ C}$  (on a hotplate) for 48 h prior to analysis. The analytical error was  $\pm 5\%$ . The upper limits of Li, Cs, and Rb were different because of differences in the type of spectrometry used.

**Table 1.** Rare-element composition (ppm) of pegmatite samples from the Boam deposit.

Sample	Location	Li	Be	Cs	Rb	Y	Nb	Sn	Ta	Analysis
BA 1	Pgt 1	>400.0	348.0	>100.0	1270.0	0.7	10.5	<1.0	2.1	Actlabs UT6 <sup>1</sup>
BA 2	Pgt 11	>400.0	20.6	>100.0	2200.0	0.5	11.3	16.0	2.4	Actlabs UT 6 <sup>1</sup>
BA 3	Pgt 5	>400.0	226	>100.0	2130.0	1.0	42.2	11.0	51.2	Actlabs UT 6 <sup>1</sup>
BAN 1	Pgt 6	589.0	26.4	82.0	203.0	2.4	0.7	6.2	<0.05	Actlabs UT 1 <sup>2</sup>
BAN 2	Pgt 7	5280.0	12.2	>500.0	>500.0	0.1	4.9	22.1	0.05	Actlabs UT 1 <sup>2</sup>
BAN 3	Pgt 3	1130.0	323.0	880.0	2250.0	0.5	20.7	60.3	66.8	KIGAM <sup>3</sup>
BAN 4	Pgt 9	2420.0	47.0	779.0	1140.0	1.4	28.7	12.5	19.1	KIGAM <sup>3</sup>

>: over the upper detection limit; <: below the detection limit; <sup>1</sup> Actlabs Ultratrace (UT) 6 code analysis; <sup>2</sup> Actlabs Ultratrace (UT) 1 code analysis; <sup>3</sup> KIGAM HR-ICP-MS analysis.

The polished REP thin-sections were studied using microscopy after macroscopic mineral and textural characterization of the rock sample. Backscattered electron (BSE)

images were obtained to examine the internal texture of the minerals using scanning electron microscopy and energy dispersive spectroscopy (SEM-EDS; JEOL JXA-8100) at Gyeongsang National University, Jinju, South Korea. BSE images were taken at 100× magnification with an accelerating voltage of 15 kV.

### 3.2. Geometric Analysis

Lee et al. [5] conducted a detailed study of the Boam deposit and grouped REPs based on their locations into the main (Boam deposit), western (c. 450 m west of the deposit), and eastern (c. 300 m east of the deposit) orebodies (Figure 1b). In this study, geometrical analysis of the individual REP bodies in these three groups (the main group was subdivided into main and submain groups for classification) was performed to determine the factors controlling the arrangement of the pegmatites developed in the limestone layer within a linear distance of approximately 1 km.

Research on the factors controlling intrusion using geometrical analysis can be integrated with the factors that control the overall arrangement. Here, we analyzed thirteen individual REP bodies including their general strike and dip, inter-relationships with surrounding fractures, and deformation characteristics (Table 2, Figure 1b). All analyses were performed in two-dimensional sub-vertical planes, and some outcrops were visualized using photogrammetry software (Metashape 1.6.2; Agisoft LLC, St. Petersburg, Russia). In the case of the pegmatites showing various intrusion planes, strike and dip were estimated based on the most dominant direction of the thickest pegmatite.

**Table 2.** Detailed information on the rare-element pegmatites (REPs) investigated in this study.

Orebody	No. of REP	Location	General Strike/Dip of REP Bodies	Description
Western orebody	Pgt 1	Upper part (altitude: 516 m)	N60° E-striking	Irregular and boudinage shaped pegmatites
Western orebody <sup>3</sup>	Pgt 2	Middle part (altitude: 468 m)	N40°–50° E-striking	Bended, bended, and lenticular pegmatites
Western orebody <sup>3</sup>	Pgt 3	Bottom part (altitude: 446 m)	N60° E/70° NW	Lenticular and branched pegmatites
Main orebody	Pgt 4	Pit 1	N60° E/60° SE	Irregular shaped and lenticular pegmatites
Main orebody <sup>1</sup>	Pgt 5	Eastern slope	N70° E/80° SE	Lenticular pegmatites
Submain orebody <sup>2,3</sup>	Pgt 6	Western part of Boam	EW/20° N	Zig-zag shaped pegmatites
Submain orebody <sup>2,3</sup>	Pgt 7	Northern part of Boam	N76° E/50° NW	Irregular shaped pegmatites
Submain orebody <sup>2,3</sup>	Pgt 8	Northern part of Boam	N60° E-striking	Lenticular pegmatites
Submain orebody <sup>2,3</sup>	Pgt 9	Northern part of Boam	N8° E/15° NW	Irregular shaped and lenticular pegmatites
Eastern orebody	Pgt 10	Pit I	EW/45° NW	Lenticular pegmatites
Eastern orebody	Pgt 11	Pit II	N70° E/62° NW	Lenticular pegmatites
Eastern orebodies	Pgt 12	Pit III	N50° E/62° NW	Lenticular pegmatites
Eastern orebody	Pgt 13	Easternmost outcrop	EW/62° NW	Lenticular pegmatites

<sup>1</sup> Around pit (remnants of small-scale mining) 1; <sup>2</sup> around the main orebody; <sup>3</sup> newly identified as part of this study.

## 4. Results

### 4.1. Lithium Mineralization

#### 4.1.1. Rare-Element Pegmatite (REP)

The western orebody (1130 to 1584 ppm Li; Lee et al. [5]; this study) is located approximately 450 m west of the main orebody (Figure 1b). No pits occur in the western orebody, and the pegmatite-intruded host rock (the Janggun Limestone Formation) is observed only on the outcrop. The host rock is composed of light-gray limestone that alternates from dark-gray to black sandy limestone. The limestone calcite appears recrystallized and white in color. The REPs lack internal zoning and are texturally homogeneous, and

the main constituent minerals are K-feldspar, quartz, plagioclase (albite), and Li minerals (spodumene, elbaite, and lepidolite). In the western orebody, purple or pink lepidolite is rarely observed while medium-grained (<2.5 cm) white or light-brown spodumene is more abundant than in the main-submain and eastern orebodies (Figure 2a).

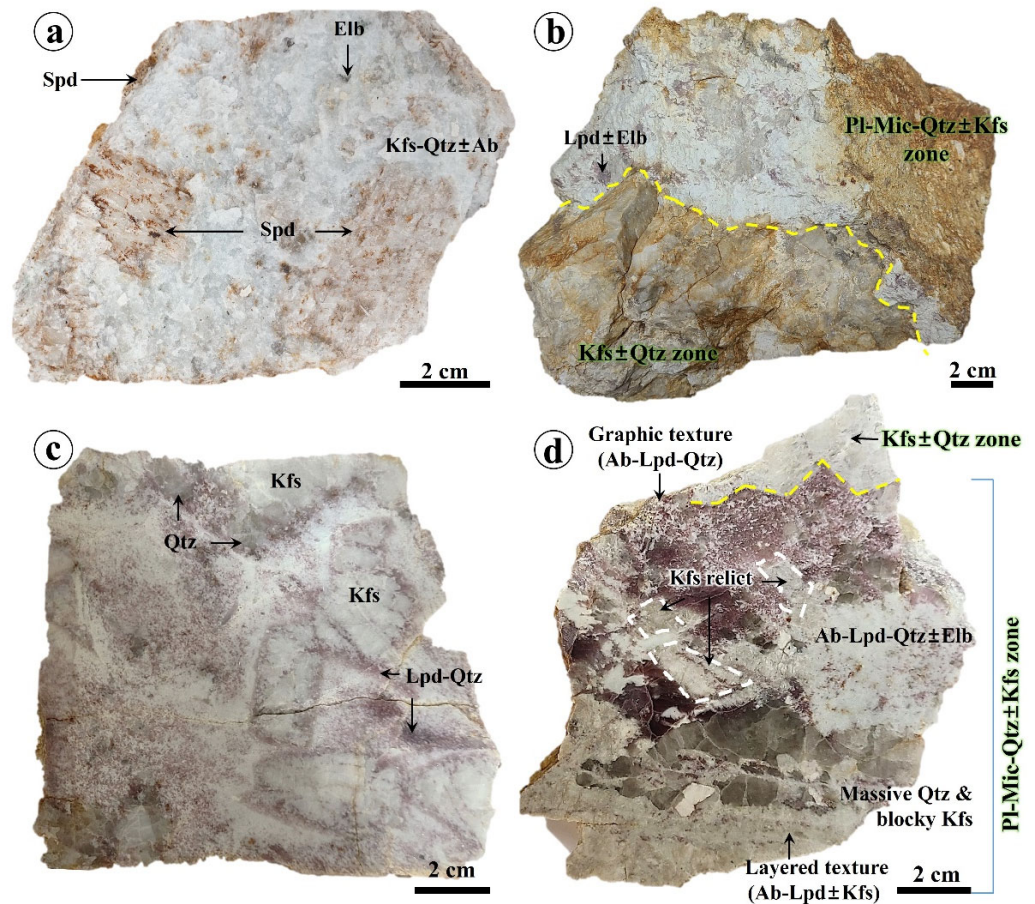


**Figure 2.** Representative rare-element pegmatite (REP) rock samples from the Boam deposit. (a) Spodumene (light brown) and blocky K-feldspar (milky white) in the western REP. (b) Internally zoned REP showing two distinct zones: a K-feldspar ± quartz zone and a plagioclase-mica-quartz ± K-feldspar zone. (c) Medium-grained (<2.5 cm) blocky K-feldspar surrounded by quartz-lepidolite-albite at the internal zone boundary. (d) Greisenized (hydrothermal altered) minerals showing pegmatite textures. Note the quartz-lepidolite-albite graphic and layered texture. Abbreviations: Ab = albite, Elb = elbaite, Kfs = K-feldspar, Mic = mica, Lpd = lepidolite, Pl = plagioclase, Qtz = quartz, and Spd = spodumene.

In the main-submain orebody (589 to 5280 ppm Li; Lee et al. [5]; this study), four small-scale pits exist (approximately 5–30 m in length and NE-trending), although some have collapsed. The host rock (Janggum Limestone Formation) is composed of light-gray limestone that alternates from dark-gray to black sandy limestone, and shows a selectively weathered structure. Some limestone is partially skarnized by pegmatite intrusions with local Fe-mineralization, although the skarnized zone is very narrow (<0.5 m). The REPs are rather inhomogeneous compared to western REPs and show internal zoning with different mineral assemblages (an inner K-feldspar ± quartz zone and an outer plagioclase-mica-quartz ± K-feldspar zone). Brecciated and/or massive Li orebodies consisting of fine-grained aggregates of lepidolite ± elbaite are only observed in the outer zone. The brecciated Li orebodies are angular or subangular and variable in size, ranging from 0.5 cm to a few centimeters. The breccia matrix is composed of albite, quartz, and minor muscovite, all of which are cross-cut by late calcite veinlets. The massive Li orebodies

consist of lepidolite, elbaite, albite, and quartz, and are partially brecciated. Spodumene is observed less commonly than in the western REPs.

The eastern orebody (4474 ppm Li; Lee et al. [5]) is located approximately 300 m east of the main-submain orebody and contains three small-scale pits (approximately 5–10 m in length and NE-trending; Figure 1b). The host rock (Janggun Limestone Formation) is composed of light-gray limestone that alternates from dark-gray to black sandy limestone and shows a selectively weathered structure. The following two internal zones are recognized within the REP based on the mineral assemblage: (1) an inner K-feldspar  $\pm$  quartz zone, and (2) an outer plagioclase-mica-quartz  $\pm$  K-feldspar zone (Figure 2b).

The inner zone is variable in thickness but is generally tens of centimeters thick. This zone mainly consists of blocky K-feldspar with minor quartz. The outer zone occurs in the upper and lower parts of the REP; these are primarily composed of albite, muscovite, and quartz. Brecciated and/or massive Li orebodies consisting of lepidolite-elbaite were observed only in the outer zone (Figure 2c,d). Medium-grained (<2.5 cm) blocky K-feldspars are observed at the internal zone boundary (Figure 2c). Massive quartz is concentrated in a specific part parallel to the internal zone boundary (Figure 2d). The albite, lepidolite, quartz, and minor K-feldspar show a graphic and layered texture in the outer zone (Figure 2d). Elbaite grains are perpendicular to the contacts of the REP and exhibit a unidirectional solidification texture (UST).

The REPs from the Boam deposit represent regional zoning from the western orebodies (Pgt 1–3) to the main-submain orebodies (Pgt 4–9) to the eastern orebodies (Pgt 10–13) based on the mineral assemblage. The main minerals of the western REPs are K-feldspar, quartz, and minor plagioclase (albite), whereas the main and eastern REPs are composed mainly of plagioclase (albite), mica, and quartz with minor K-feldspar. Spodumene, which is the main Li mineral in the western REP intergrowth, is rarely observed in the main-submain and eastern REPs. Lepidolite (Li-mica), which is rarely observed in the western REP, occurs in greater amounts in the main-submain and eastern REPs.

#### 4.1.2. Minerals in Rare-Element Pegmatites (REPs)

The REPs from the western orebody lack internal zoning and are texturally homogeneous but become internally zoned with increasing distance from the western to eastern orebody based on the mineral assemblage.

The fine-grained (<2.5 cm) blocky K-feldspar shows a perthite texture and is mainly present in the homogeneous REP and inner zone of the REP as a primary mineral. These K-feldspar grains are mostly replaced by saccharoidal albite in the outer zone of the REP (Figure 3a,b). The milky to grey quartz is variable in size but coarser in the outer zone of the REP.

The euhedral to subhedral plagioclase is mostly albite, showing albite twinning. These albites are the most abundant minerals in the internally zoned REPs (Figure 3a,b). The primary plagioclase in the homogeneous REP shows an igneous texture and intergrowth with K-feldspar, quartz, and spodumene. In contrast, secondary plagioclase in the zoned pegmatite with saccharoidal texture has replaced the K-feldspar and coexists with mica (Figure 3b). The amount of albite locally increases from the homogeneous REPs to internally zoned REPs, and from the inner zone to the outer zone.

White to green muscovite is abundant in the outer zone of the REP. Muscovite has one perfect cleavage, often with minor bending (muscovite fish); the observed muscovite is intergrown with recrystallized quartz and replaces both the K-feldspar and plagioclase (albite) (Figure 3b,c). The BSE images show that the rims of the muscovite in a large number of the samples are enriched with rare elements such as Cs (Figure 3d).

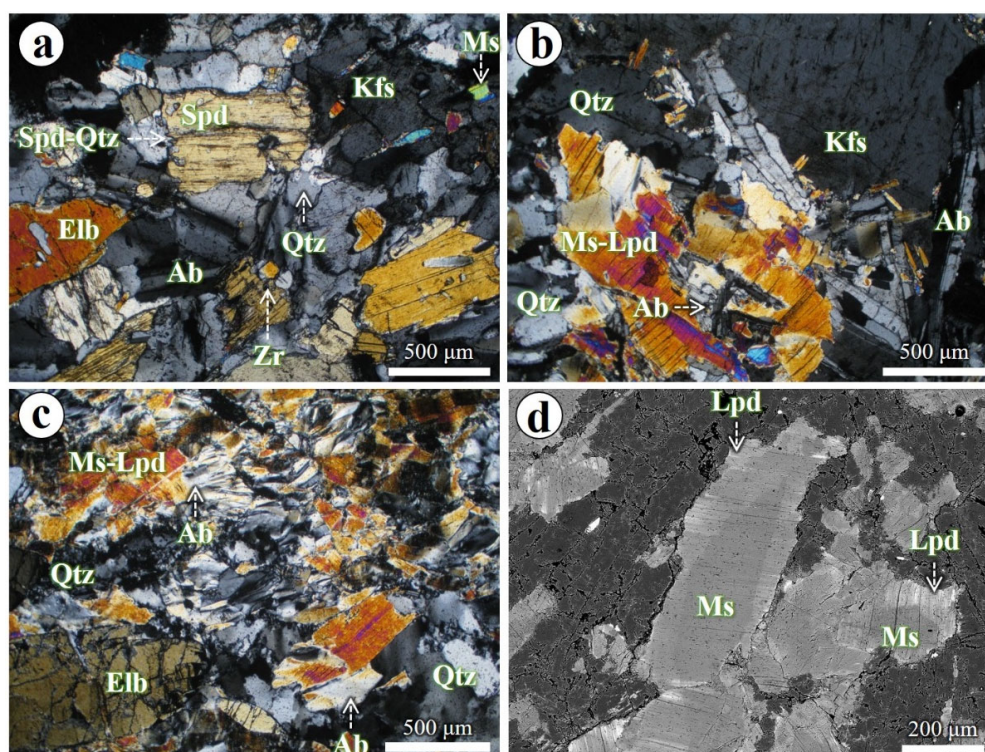


**Figure 3.** Photomicrograph of Li minerals from the Boam deposit. (a) Spodumene intergrowth with magmatic minerals such as K-feldspar, quartz, and plagioclase (albite) (under cross-polarized light). (b) K-feldspar replaced by saccharoidal albite (under cross-polarized light). (c) Muscovite intergrowth with recrystallized quartz and replacing both K-feldspar and plagioclase (under cross-polarized light). (d) Backscattered electron (BSE) image of muscovite-lepidolite. Abbreviations: Ms = muscovite. See Figure 2 for other abbreviations.

White to pale-brown spodumene crystals up to several centimeters are present and are more abundant in the homogeneous REP than in the internally zoned REP. The spodumene grains are typically subhedral tabular or lath-shaped, often with symplectitic intergrowth with quartz along the grain boundaries (Figure 3a). The spodumene is intergrown with magmatic minerals, such as K-feldspar, quartz, and plagioclase (albite) (Figure 3a), and these grains contain magmatic zircons that are interpreted as primary inclusions.

The acicular to prismatic elbaite grains are pale-green to pink, and are observed in all the REPs from the Boam deposit. The elbaite is intergrown with lepidolite or cross-cut lepidolite (Figure 3c). The main Li mineral in the internally zoned REP (Figure 3b–d) is lepidolite, which is macroscopically purple to violet and forms variably sized, platy to irregular-shaped grains. The lepidolite replaces muscovite and mainly occurs in the outer zone of the REP (Figure 3d). These lepidolites are broken into thin flakes or bent in the brecciated REP (main-submain orebodies). Fluorite, apatite, zircon, and beryl are accessory minerals within the REP.

The western homogeneous REP is enriched in K-feldspar, and spodumene is the main Li mineral. However, with increasing distance from west to east, the REPs are internally zoned, the relative proportion of albite to K-feldspar gradually increases, and the amounts of muscovite and lepidolite also increase.

#### 4.2. Geometry of the Rare-Element Pegmatite (REP) Bodies

Thirteen REP bodies, from west to east, are described in the following sections.

#### 4.2.1. Western REP Bodies

The western REP bodies are located approximately 450 m to the west of the main REP bodies, and we identified two new sets of REP bodies by tracing the ENE–WSW-trending downward profile (Figure 4). The three sets of REP bodies were divided into upper (Pgt 1), middle (Pgt 2), and bottom (Pgt 3) parts based on their elevation; the connectivity of these REP bodies was difficult to identify because of the thick soil cover. One set of REP bodies (Pgt 1) was identified in the nodular limestone at an altitude of 516 m (Figure 4a). The eastern Pgt 1 body is composed of more than two lenticular bodies arranged parallel to the  $N60^{\circ}E/70^{\circ}NW$ -striking bedding, with a maximum thickness of approximately 20 cm. The western Pgt 1 body has a variable thickness with an irregular shape and highly fractured host rock. The weakly deformed bedding planes (with no distinct folding, brecciation, densely spaced (<10 cm) fractures, or faulting) near the REP bodies are mostly parallel to the intrusion planes.

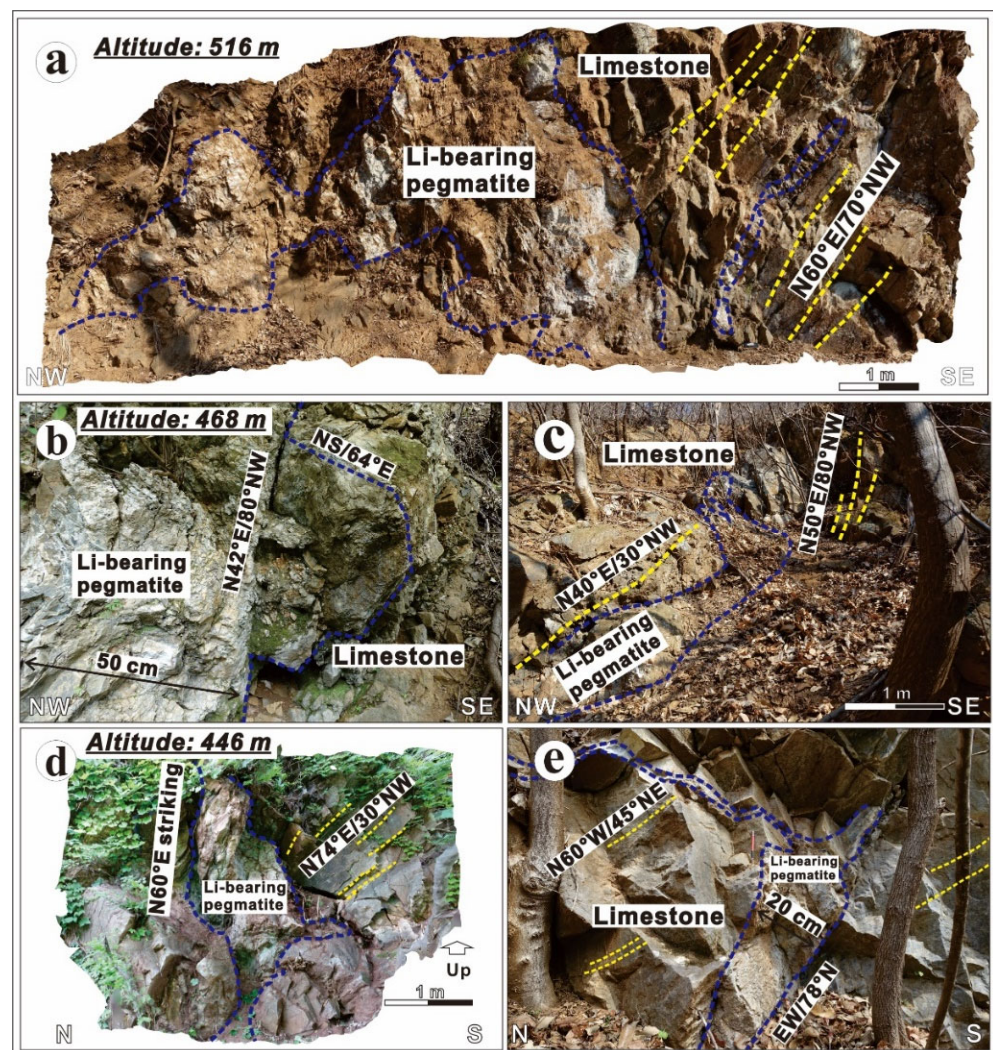


**Figure 4.** Upper (Pgt 1), middle (Pgt 2), and bottom (Pgt 3) parts of the western rare-element pegmatite (REP) bodies. The boundaries of the bodies are highlighted with thick blue dotted lines, and the beddings are highlighted with thick yellow dotted lines. (a) Pgt 1 is composed of an irregular body and more than two lenticular bodies. (b,c) Pgt 2 is composed of two REP bodies parallel to the bedding and is branched or bent by a N–S-striking fracture and rotation of the bedding, respectively. (d,e) Pgt 3 consists of two REP bodies that cross the bedding, with thin REP bodies branching along the bedding. Yellow and blue dotted lines indicate beddings and orebody contacts, respectively.

Another set of REP bodies (Pgt 2) was identified in the nodular limestone at an altitude of 468 m east-northeast of Pgt 1 (Figure 4b,c). The eastern Pgt 2 body shows a branched shape with a maximum thickness of approximately 50 cm (Figure 4b). Although the dominant strike of the body is N42E and parallel to the bedding, the pegmatite branches into the fracture at the point of intersection with the N–S-striking fracture. The western Pgt 2 body has a planar shape with a blunt-ended tip and a maximum thickness of approximately 70 cm (Figure 4c). This body is intruded parallel to the bedding and is slightly bent by the local rotation of the bedding. Both bodies are lenticular, and the extension to the upper part disappears on the outcrop.

The third set of REP bodies (Pgt 3) occurs in the nodular limestone and marble at an altitude of 446 m in the east-northeast area of Pgt 2 (Figure 4d,e). The eastern Pgt 3 body is lenticular with a maximum thickness of approximately 120 cm (Figure 4d). This body intrudes the bedding, with some thin (<10 cm) REP bodies branching into the bedding. Similarly, the western Pgt 3 body is lenticular, has a maximum thickness of approximately 20 cm (Figure 4e), and intrudes the bedding as thin (<10 cm) REP bodies. The upper extension of the Pgt 3 set is obscured by vegetation.

The characteristic intrusive patterns observed in Pgt 1 can be interpreted as follows (Figure 4a): (1) the eastern Pgt 1 body shows a boudinage structure (the upper body is continuous with necks); and (2) the irregular Pgt 1 set is difficult to interpret based on the exposed surface of this outcrop, but we identify the following three possibilities: (i) asperity of the exposed surface, (ii) post-deformation of intrusions, and (iii) fingers of sill. Three-dimensional observations would aid a more accurate interpretation.

The factors controlling the intrusion of the western REP bodies (Pgt 1–3) are bedding, N–S-striking fracturing (i.e., branching), and N60E- or E–W-striking discontinuities (i.e., dykes). Although the exact thickness was not measured for Pgt 1, Pgt 2, and Pgt 3 showed similar degrees of dilation with a total thickness of 120 and 140 cm, respectively.

#### 4.2.2. Main REP Bodies

Three pits were identified in the Boam deposit and two REP bodies (Pgt 4 and Pgt 5) were visually confirmed. Pgt 4 (near the deposit entrance) can be confirmed as a mining trace in pit 1, whereas Pgt 5 is observable only on the slope near pit 3 (note that pits 2 and 3 have collapsed). Thus, we inferred the geometry of Pgt 5 from the relationship between the body and the surrounding structures. To explain each REP body, the western slope (around pit 1) and the eastern slope (around pits 2 and 3) are described separately.

We identified a mixture of brecciated Pgt 4 and the host rock (limestone) in the N80° W/60° NE-striking fault zone (approximately 30 cm thick) and the western slope of the pit 1 entrance (Figure 5a). Densely developed N15° E-striking fractures crosscut the N82° W/20° NE-striking beddings on the eastern slope of the pit 1 entrance, although these fractures do not penetrate the fault zone. In the mine, a N60° E/60° SE-striking lenticular-shaped REP body (Pgt 4) was confirmed (Figure 5b). This body cuts the N84° W/20° NE-striking bedding with a maximum thickness of approximately 1 m. The intrusive plane is relatively sharp and fragments (i.e., xenoliths) of the host rock are captured within the pegmatite body.

A brecciated REP body exists around the entrance of the pit, whereas a massive REP body was confirmed in the mine (Figure 5). We attribute this difference in deformation to the N80° W/60° NE-striking fault. A detailed analysis of this fault is required because it may redistribute the location of the REP body, although this is made difficult because the key bed in the footwall could not be found, possibly having been eroded. We consider that the factors controlling Pgt 4 are the ENE–WSW-striking discontinuity and (post-intrusion) faulting.

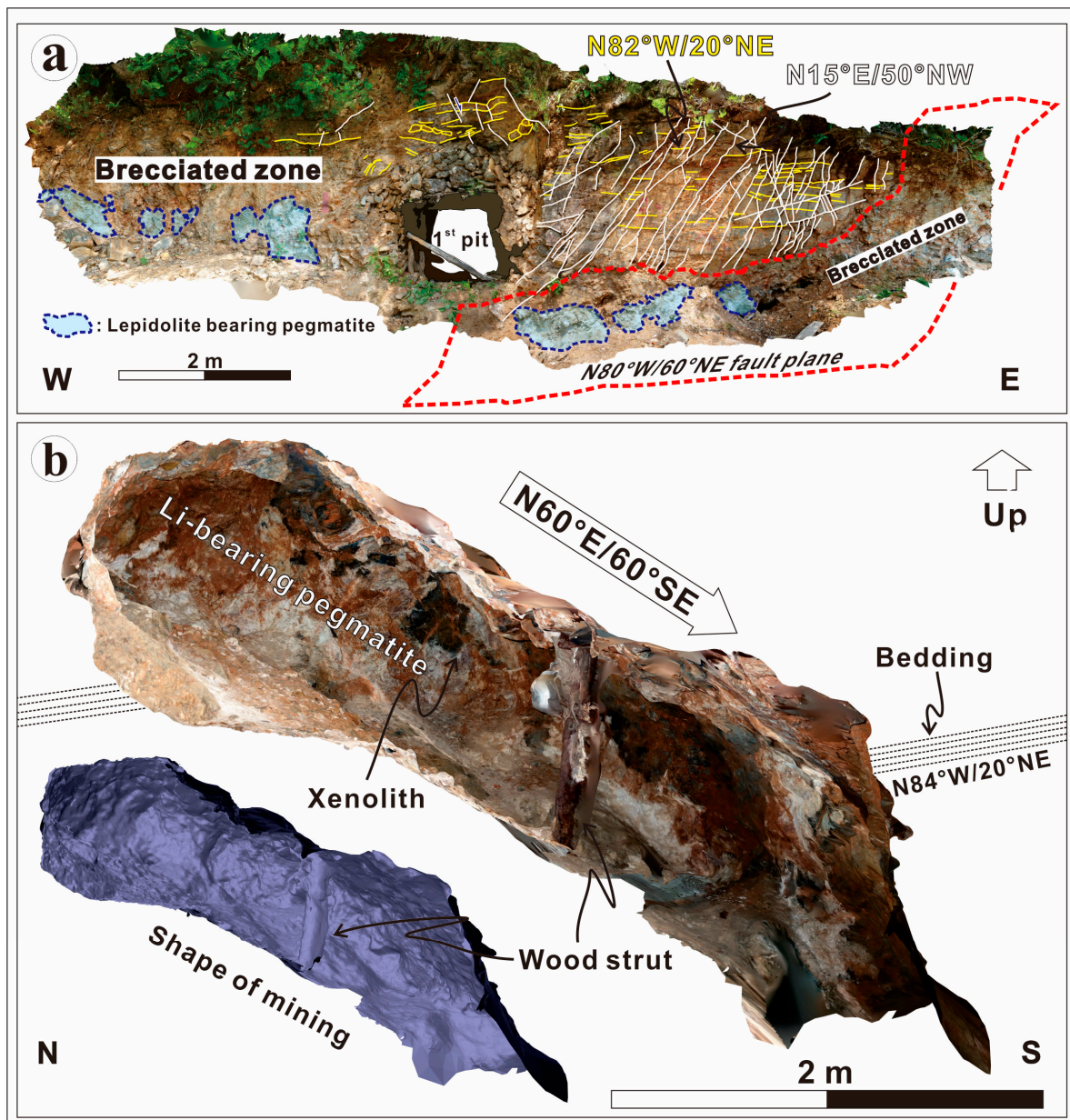


**Figure 5.** Western slope and rare-element pegmatite (REP) bodies (Pgt 4, pit 1) of the Boam deposit. (a) Brecciated host rock and REP body mixed in the N80° W/60° NE-striking fault zone and on the slope. White dotted lines indicate fractures. (b) Lenticular and N60° E/60° SE-striking Pgt 4 in the pit cross-cutting the bedding. The solid image generated using Agi software shows the shape of the mine.

The eastern end of the western slope (near pit 2) collapsed in the N80° W/60° NE-striking fault zone (Figure 6a). The N30° W- and NS-striking fault sets between pits 2 and 3 have caused local rotation of the bedding and displaced the bedding of the hanging wall downward. Pgt 5 is planar, with a maximum thickness of approximately 30 cm (Figure 6b). A N70° E-striking REP body cross-cutting the bedding extends from pit 3 to the top of the slope with a 45° dip until it runs into the N74° W/80° NE-striking fault. The body of the relatively northern block, based on the fault, falls downward (Figure 6c). From the fault zone to the east, the following features were identified: (1) the host rock and REP body are brecciated, (2) the fracture density and the irregularity of the REP body shape increase, and (3) the slopes are eventually only occupied by boulders of the host rock and the REP body.

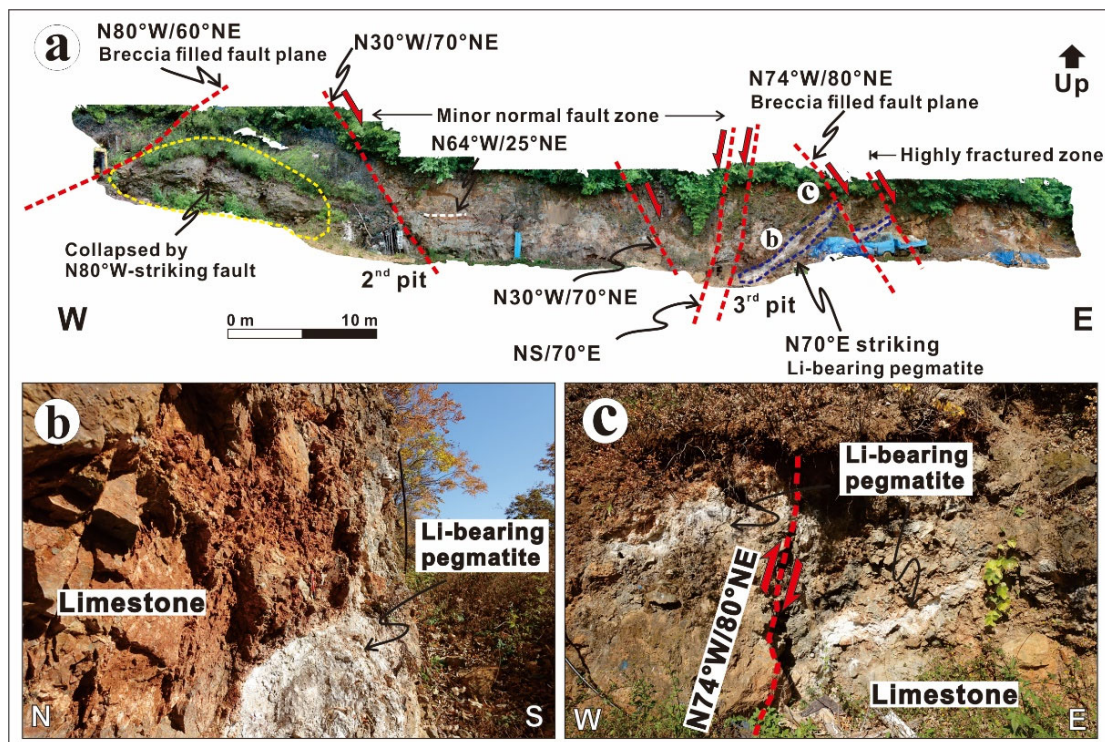


**Figure 6.** Eastern slope and rare-element pegmatite (REP) bodies (Pgt 5, around pit 3) of the Boam deposit. (a) Access to pits 2 and 3 is restricted owing to collapse, and the western side of pit 2 has collapsed as a result of the N80° W/60° NE-striking fault. The N–S- and NW–SE-striking faults developed between the two pits. (b) An N70° E-striking REP body is observed on the upper slope of pit 3. (c) The N74° W/80° NE-striking fault has displaced Pgt 5 (northern block down).

The fault zones observed on the western slope can be interpreted as follows (Figure 6a): (1) N30° W- and N–S-striking faults are interpreted as normal faults, evidenced by downward displacement of bedding on the hanging wall. Based on the amount of displacement, the N30° W-striking fault (<20 cm dip separation) is interpreted as a subsidiary fault of the N–S-striking faults (>20 cm dip separation). Although there is no direct evidence between Pgt 5 and the fault, it is possible that the elevation difference between pits 2 and 3 is caused by this fault; (2) The N74° W/80° NE-striking fault displaced Pgt 5 and shows a wide damage zone (approximately 2 m), although there are no kinematic indicators of horizontal movement in the key beds. As the faults interpreted as post-intrusion deformation are important for tracing the REP bodies in the study area, these require more detailed interpretation. Overall, the factors controlling Pgt 5 are interpreted as being linked to ENE–WSW-striking discontinuities and (post-intrusion) faulting.

The REP bodies (Pgt 4 and Pgt 5), faults, and breccia zones observed in the Boam deposit are shown in Figure 7. The ENE–WSW-striking REP bodies (Pgt 4 and Pgt 5) show a sub-parallel arrangement, and the WNW–ESE-striking faults crosscut both REP bodies. Brecciated and collapsed zones (boulder zones) are distributed around the fault zones. Owing to the collapse of the slope and mines, the relationship between the REP bodies and the existence of other REP bodies could not be confirmed, although we interpret this arrangement as being indicative of two or more sub-parallel REP bodies in the Boam deposit.

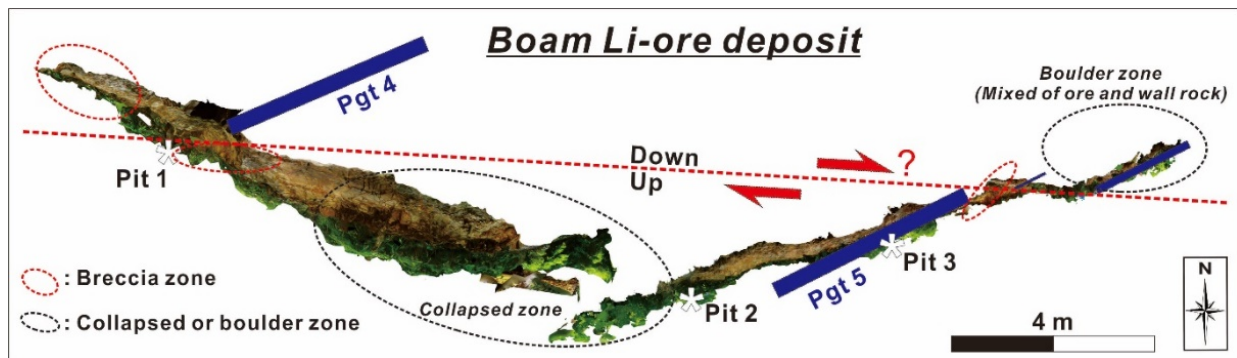


**Figure 7.** Map of the main rare-element pegmatite (REP) bodies of the Boam deposit. REP bodies Pgt 4 and Pgt 5 are highlighted with thick blue lines, and the WNW–ESE-striking fault is shown by a red dotted line. Breccia zones and collapsed (or boulder) zones are highlighted by red and black dotted circles, respectively.

#### 4.2.3. Submain REP bodies

Four REP bodies (Pgt 6–9) were identified near the main REP bodies, described here sequentially from west to northeast.

One REP body (Pgt 6) was identified in the nodular limestone at a small open pit (Figure 8). Pgt 6 is zig-zag shaped with a maximum thickness of approximately 1 m. The EW/20° N-striking bedding is mostly planar but slightly folded near the sub-vertical intrusion plane (Figure 8a). N–S-striking fracture sets also occur with cross-cut bedding.

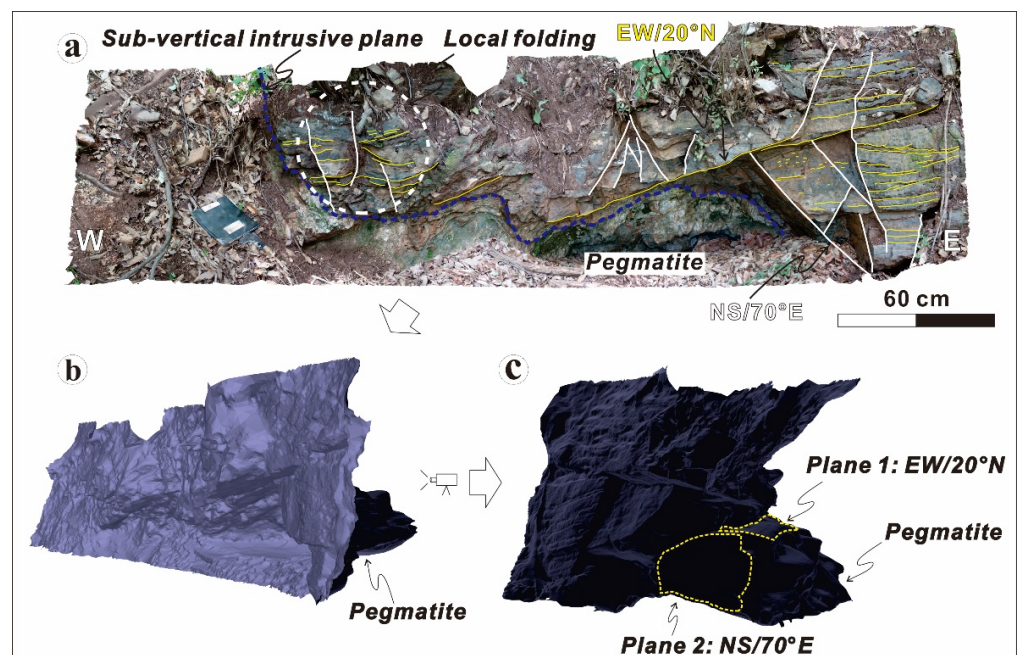


**Figure 8.** Rare-element pegmatite (REP) body Pgt 6 in a small open pit. (a) The REP body is zig-zag shaped with EW/20° N-striking bedding and NS/70° E-striking fractures. (b,c) Solid images produced using Agi software. The mine shape shows the interrelationship between bedding and fractures.

We did not identify any displacement or deformation of the host rock or pegmatites by the N–S-striking fractures, and local folding around the vertical intrusion plane—especially near the fracture plane—is interpreted as being caused by intrusion (i.e., dragging; Figure 8a). Therefore, the N–S-striking fractures are interpreted as pre-dyking fractures.

The back images of the pits (produced using Agi software) further illustrate that the pegmatite intrusion pattern is controlled by the bedding and fractures (Figure 8b,c).

REP bodies (Pgt 7) showing both irregular and sharp intrusive planes in the nodular limestone were identified in the outcrop (Figure 9a,b), with an inferred maximum thickness of approximately 4 m (the exact intrusion direction was ambiguous). The intrusive plane of Pgt 7 can be divided into southern, upper, and northern planes, which have the following characteristics: (1) the upper part of the southern intrusive plane is parallel to the  $N70^{\circ}W/70^{\circ}$  SW-striking bedding, whereas the lower part is deflected into the  $70^{\circ}W/30^{\circ}$  NE-striking fractures (Figure 9c); (2) the upper intrusive plane is zig-zag shaped; (3) the northern intrusive plane is parallel to the  $N76^{\circ}E/50^{\circ}$  NW-striking bedding (Figure 9d). Notably, the bedding dip direction has changed from north to south, and some southern bedding is intruded by thin pegmatites (<10 cm). The  $N70^{\circ}W/30^{\circ}$  NE-striking fractures and a highly fractured zone in the host rock are filled with calcite veins.

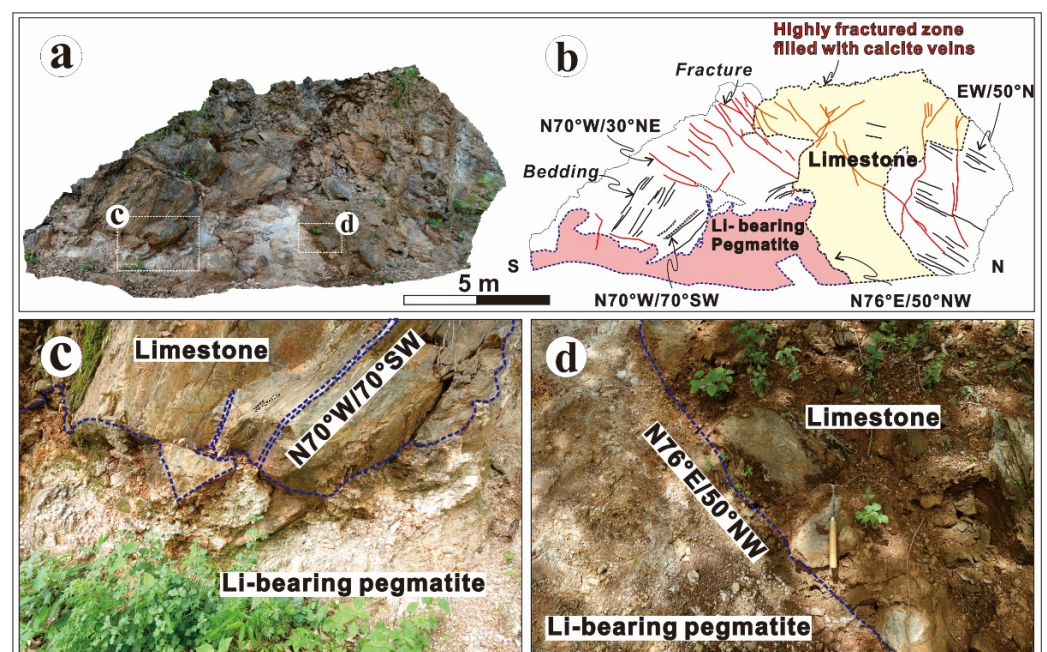


**Figure 9.** Rare-element pegmatite (REP) body Pgt 7 in the limestone outcrop. (a,b) Pgt 7 is irregularly shaped, the host rock is highly fractured, and the bedding is folded based on the REP body. (c) The southern boundary is bent, and a thin REP intrudes along the bedding. (d) The northern boundary lies parallel to the bedding.

The irregular shape of the upper and southern intrusive plane is interpreted as the refraction of the REP bodies due to the intersection of the bedding and the  $N70^{\circ}W/30^{\circ}$  NE-striking fracture; there is no visible displacement or deformation of the rocks or the northern intrusive plane by the fractures (Figure 9b,c). Folding (anticline and fold axis =  $44^{\circ}/N48^{\circ}W$ ), indicated by the opposite dipping direction of the bedding, is also interpreted as being related to intrusion because there are no kinematic indicators or structures related to folding in the rocks. Such a folded structure does not appear in the surrounding rocks, which supports the possibility of local folding related to intrusion. Therefore, it is likely that local folding (non-tectonic folding) occurred when the pegmatite intruded, and, later, calcite veins developed along the highly fractured hinge zone.

REP body Pgt 8 was identified in the nodular limestone outcrop (Figure 10). Although only a small part was exposed, Pgt 8 shows a lenticular shape with a maximum thickness of approximately 50 cm (Figure 10a,c). The northern part of Pgt 8 is bordered by a  $N64^{\circ}W/90^{\circ}$ -striking fracture, and the southern part is covered by a layer of host rock (Figure 10b,c). The bedding around this REP body is relatively consistent with an  $EW/50^{\circ}N$  strike, although

the bedding overlying the exposed pegmatite rotates locally in the  $N60^{\circ} E/50^{\circ} SE$  direction (Figure 10a).

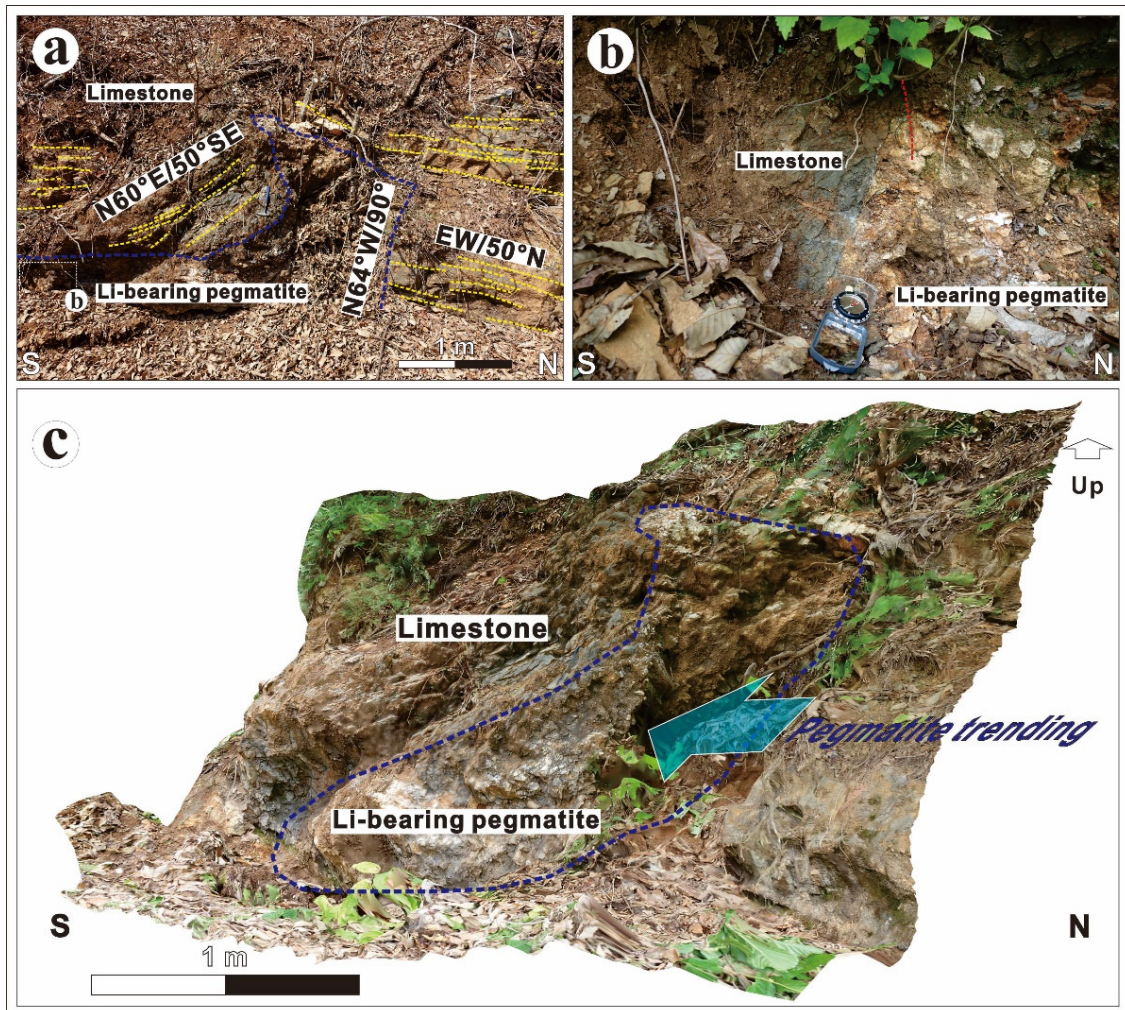


**Figure 10.** Rare-element pegmatite (REP) body Pgt 8 developed in the outcrop. (a) The bedding changes from an EW/50° N strike to a  $N60^{\circ} E/50^{\circ} SE$  strike where the REP body is exposed. The  $N64^{\circ} W/90^{\circ}$ -striking fracture is bound to the northern part of the body. (b) The limestone layer overlies the pegmatite. (c) The direction of the pegmatite intrusion is parallel to the bedding of the overlying limestone.

The factors controlling Pgt 8 are the  $N64^{\circ} W/90^{\circ}$ -striking fractures and the  $N60^{\circ} E/50^{\circ} SE$ -striking bedding. Comparatively, it was difficult to confirm this relationship with Pgt 7 due to soil and vegetation cover.

REP body Pgt 9 was identified in a small pit comprising nodular limestone (Figure 11). Similar to Boam pit 1, the rocks in this pit show differences in their degree of deformation. Firstly, a weakly deformed zone was identified inside the pit, and planar and massive REP bodies were observed parallel to the N–S-striking bedding (Figure 11a,c,d). The N–S-striking bedding not only provided a conduit for the planar REP body but also arrested the extension of the upside of the REP body (Figure 11a,c). Secondly, a highly deformed zone was identified around the pit entrance, and a mixture of the brecciated irregular Pgt 9 REP body and the host rock was observed (Figure 11b,d–f). The dominant strike of the bedding is NW–SE-trending.

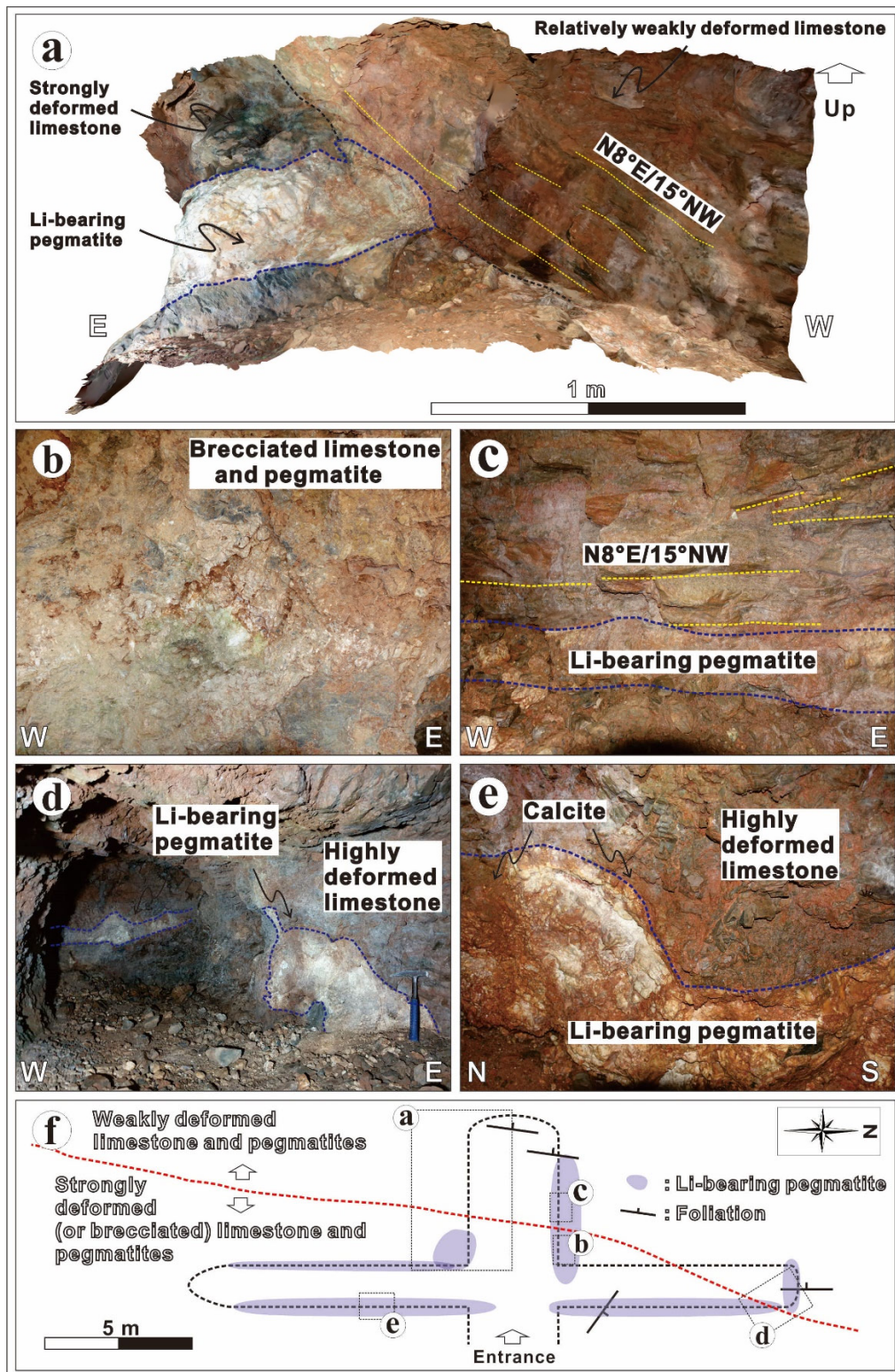


**Figure 11.** Rare-element pegmatite (REP) body Pgt 9 developed at a small pit. (a) Pgt 9 developed in strongly deformed limestone and its extension is controlled by the bedding of weakly deformed limestone. (b,c) Although the rocks were on the same wall, a difference in the degree of deformation was observed. (d,e) In the N–S plane, strongly deformed rocks were observed, whereas in the E–W plane, relatively weakly deformed rocks were observed. (f) The location of each figure is marked on the simplified map of the pit. NNE–SSW-trending lines were inferred based on the differences in the degree of deformation.

As a result of plotting these elements on a simplified map, we established the NNE–SSE-trending boundary based on the difference in deformation between the eastern weakly deformed zone and the western strongly deformed zone (Figure 11f). The boundary in the pit could not be accurately evaluated because it was not clearly recognized. Nevertheless, it is likely that redistribution of the orebody or asymmetric deformation occurred at this boundary, which requires further investigation.

#### 4.2.4. Eastern REP Bodies

The eastern REP bodies are located approximately 300 m east of the main REP bodies (Figure 12). Three pits (pit I to the west, Pgt 10–12) and one outcrop (Pgt 13) were identified in the limestone, although for safety reasons, investigations were not performed inside the pit.

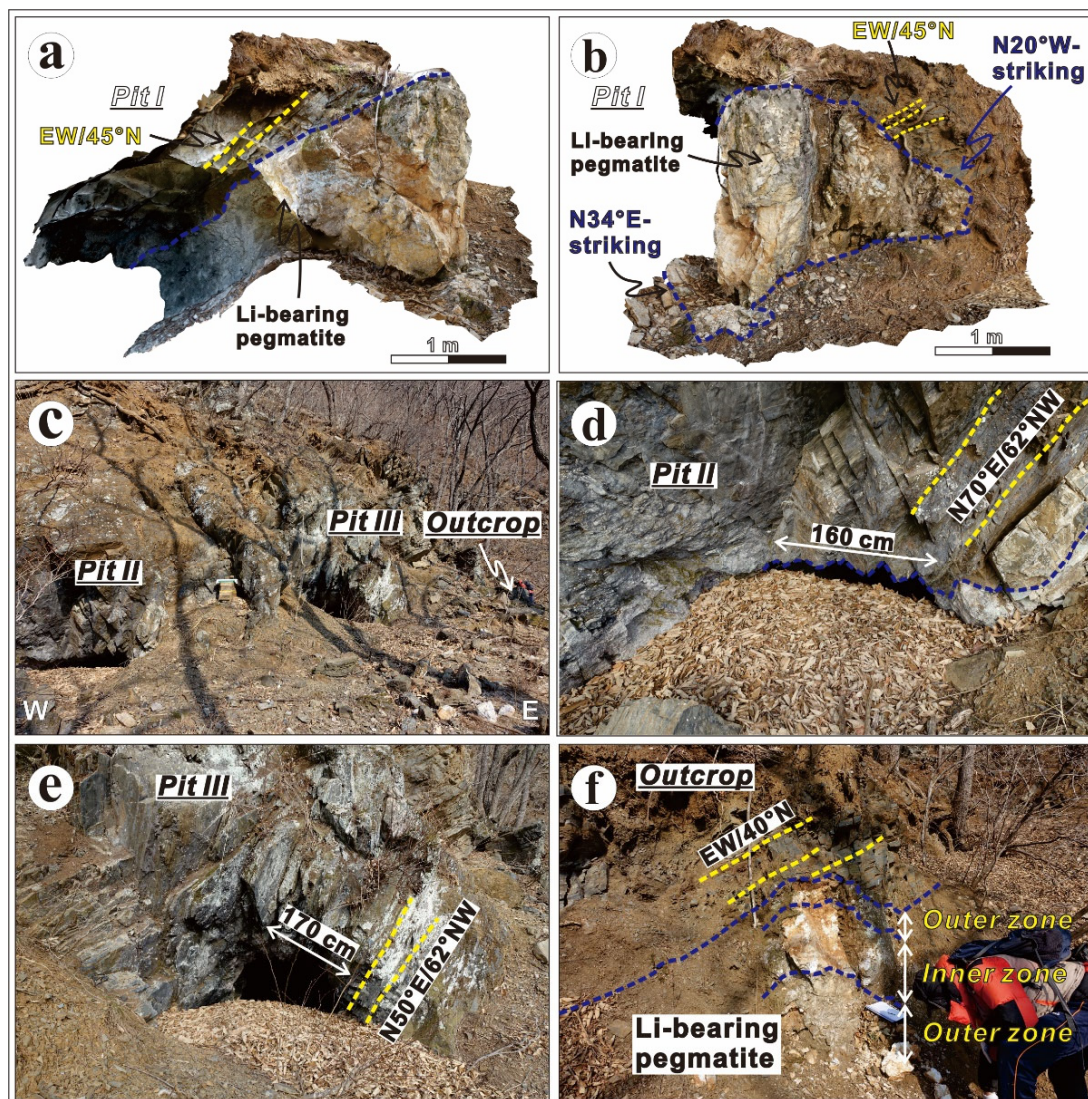


**Figure 12.** Pit I (Pgt 9), pit II (Pgt 10), pit III (Pgt 11), and outcrop (Pgt 12) of the eastern rare-element pegmatite (REP) bodies. (a,b) The long axis of Pgt 9 is parallel to the bedding, while the short axis is lenticular owing to discontinuities and rotation of the bedding. (c) Positions of pit II, pit III, and outcrops. (d,e) Pgt 10, Pgt 11, and Pgt 12 show the intrusion pattern parallel to the bedding, and the excavation extension of each pit is approximately 10 m (f) Outcrop (Pgt 13) showing the internal zoning.

The massive and lenticular REP body Pgt 10 is sub-parallel to the EW/45° N-striking bedding identified in pit I (Figure 12a,b). At the pit entrance, the intrusive plane is bent owing to the rotation of the N34° E-striking bedding, and the lateral extension is controlled by a N20° W-striking intrusion plane crosscutting the bedding. Pgt 11 and Pgt 12, which develop in pit II and III, respectively, show similar intrusion patterns parallel to the bedding, and thin pegmatites (<10 cm) were also observed to intrude the bedding (Figure 12c–e). Pgt 13 in the outcrop intrudes along the EW/40 N-striking bedding, although characteristic intrusion patterns were not identified owing to limited exposure (Figure 12c,f).

We interpret these REP bodies as having intrusion patterns controlled by the discontinuities that cut across the bedding as well as local bedding rotation, although the main direction of extension (i.e., the long axis) is controlled by the bedding itself (Figure 12). The main extension is interpreted as an arrangement of individual lenticular REP bodies because the pits are not connected and the excavation distance is approximately 10 m. This arrangement indicates either the intrusion of lenticular bodies into each layer, fingers of sill, or an en échelon array in the shear zone. To confirm this, a three-dimensional analysis is required.

### 5. Discussion

#### 5.1. Regional and Internal Zoning of Rare-Element Pegmatite (REP)

Most of the Li mineralization in the Boam deposit is associated with REP, which shows the following regional and internal zoning (Figure 13).

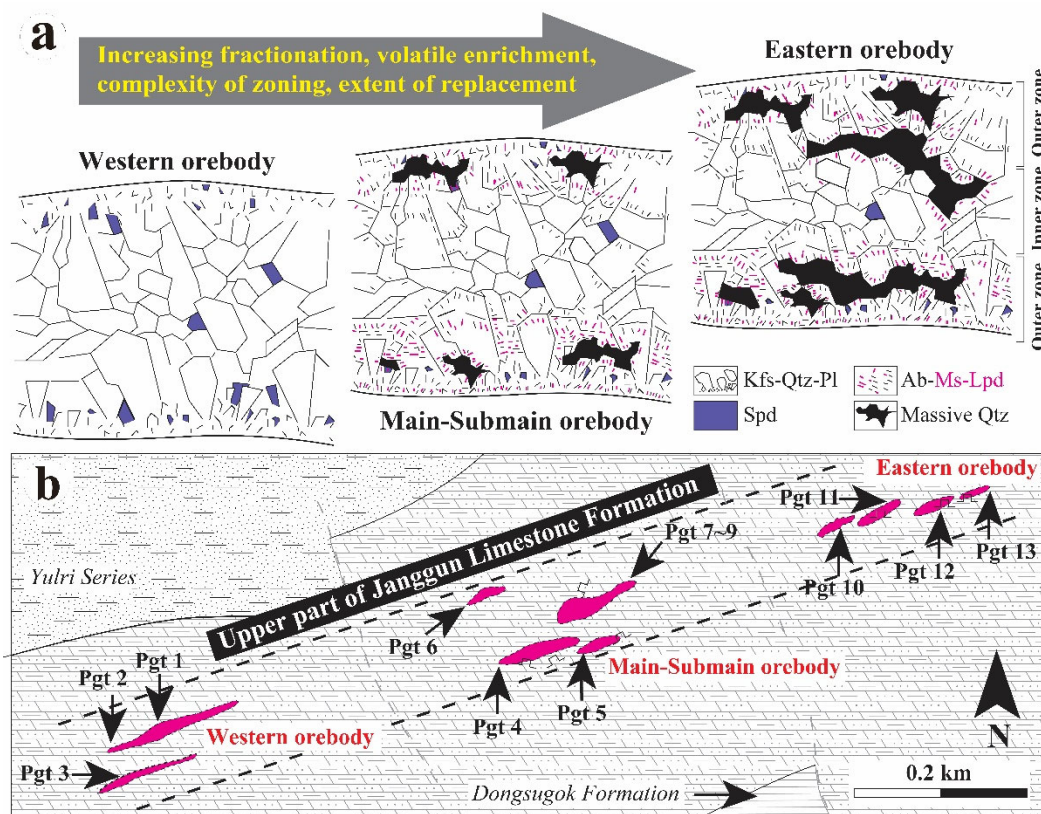


**Figure 13.** Schematic illustrations of rare-element pegmatite (REP). (a) Internal zoning (modified from [25]). The black dotted line is albite and the purple dotted line is muscovite or lepidolite. Note the inner (K-feldspar ± quartz) zone and outer (plagioclase-mica-quartz ± K-feldspar) zone. (b) Distribution of REPs in the Boam deposit. The black dotted line indicates the area with a high potential for mineral exploitation. See Figures 2 and 3 for abbreviation definitions.

(1) Regional zoning: Based on their mineral assemblages, the Boam REPs show regional zoning from the western REPs (Pgt 1 to Pgt 3) to the main-submain REPs (Pgt 4 to Pgt 9) and to the eastern REPs (Pgt 10 to Pgt 13). The main minerals in the western REPs are K-feldspar, quartz, and minor plagioclase (albite). Mica and albite, which are rarely observed in the western REPs, occur in greater amounts in the main-submain and eastern REPs. This regional zoning is characteristic of REPs. The pegmatite group outward from the fertile granite is initially enriched in K-feldspar (in the western orebody; [25]), but with increasing distance from the fertile granite and with increasing chemical fractionation of the pegmatite group, the relative proportion of albite to K-feldspar gradually increases. Indeed, the most evolved and distal pegmatites are the albite-lepidolite subtypes of the rare-element class of pegmatites in the main-submain and eastern [25,26]. World-class REPs such as the Tanco deposit in Canada are also mineralogically and texturally zoned because of the extreme differentiation in granitic melts, with rare minerals including B, Li, F, and P formed in the latest stage of crystallization [27,28].

(2) Internal zoning: The REPs show internal zoning with increasing distance from the western to eastern based on their mineral assemblages. This internal zoning is related to the evolutionary history of the REPs. The evolution of REPs in the Boam deposit can be subdivided into two stages based on the paragenetic sequence. First is the magmatic stage, with K-feldspar, quartz, plagioclase (albite), muscovite, and spodumene ( $\pm$ zircon and apatite). Second is the internal greisen (hydrothermal alteration) stage, with albite, quartz, muscovite, lepidolite, and elbaite ( $\pm$ fluorite).

The magmatic stage minerals formed a K-feldspar  $\pm$  quartz zone in the REP body (inner zone). Spodumene is intergrown with magmatic minerals, such as K-feldspar, quartz, and plagioclase (albite). This implies that spodumene from the Boam deposit occurred during the magmatic stage. With an increasing crystallization of pegmatite, the fluxing components ( $H_2O$ , B, P, and F) and rare alkalis (Li, Rb, and Cs) that are incompatible with quartz and K-feldspar become relatively enriched in the residual liquid. These flux-rich liquids are mostly sodic and contain substantially higher  $H_2O$  concentrations because of the accumulated effects of B, P, and F [29–31]. The abundance of albite in the outer zone of the REPs from the Boam deposit suggests they were albitized by sodic residual liquid (Figure 13a). Albitization leads to a decrease in the alkali/H + ratio (acidic magmatic fluid), which in turn induces the destabilization of K-feldspar and plagioclase and the replacement of these minerals by muscovite and quartz (i.e., internal greisen; [32]). During this internal greisen stage, the plagioclase–mica–quartz  $\pm$  K-feldspar zone was formed in the REP body (outer zone). In the late stages of internal greisen formation, lepidolites were formed via the replacement of muscovite (Figure 3d).

Despite recognition by a number of researchers that Li mineralization in the Boam deposit is restricted to REP bodies, some have concluded that the Li-forming fluid was derived from other hidden intrusions on the basis of greisenization and brecciation [18]. Greisenization can occur in both granitic rock and pegmatites, and greisenized pegmatites are common [28–34]. Although Li mineralization in the Boam deposit is related to greisen, the Li-forming fluid was derived from crystallized pegmatite and not from other hidden intrusions. Indeed, no evidence of Li mineralization related to hydrothermal inflow from the outside was observed in any of the REPs. The minerals occurring during the internal greisen stage (i.e., quartz, albite, lepidolite, and elbaite) show pegmatite-like textures (i.e., graphic and layered lepidolite-albite, massive quartz layers, etc.) and form internal zoning structures in the pegmatite bodies (Figure 2b,d). The similar ages of the lepidolite based on K-Ar dating ( $169.3 \pm 3.2$  to  $154.6 \pm 3.1$  Ma; Lee et al. [5]; Choi et al. [18]) and the Li orebody based on zircon U-Pb dating ( $174.5 \pm 1.4$  to  $139.8 \pm 1.2$  Ma; KIGAM [35]) extracted from spodumene (magmatic Li pyroxene) indicate that Li-forming fluid was associated with the REPs.

The textures, mineral assemblages, and geochemical characteristics of the REPs in the Boam deposit correspond to pegmatite-hosted Li deposits. Pegmatite- and granite-hosted Li greisen deposits differ with respect to their mineral exploration methods. Pegmatite-

hosted Li deposits typically show mineralogical and geochemical zoning (regional zoning), which is broadly concentric surrounding an exposed or granitic pluton [25,36]. Pegmatite intrusions with the highest economic potential for Li-Cs-Ta deposits show regional zoning up to 10 km from the parent granite [19]. In comparison, granite-hosted Li greisen deposits develop within an almost consolidated granitic body (typically the upper parts) and adjacent host rocks [37]. To efficiently explore Li resources in the Uljin area, including the Boam deposit, investigations of regional-scale pegmatite zoning from west to east should be conducted first, and an exploration plan should be designed according to the degree of pegmatite differentiation.

### 5.2. Distribution and Factors Controlling Rare-Element Pegmatites (REP)

Pegmatites arise as segregations near the roofward contact of the source pluton and lenticular or planar intrusive bodies where dyke swarms emanate from their plutons into surrounding igneous and metamorphic rocks, and where the sources are not exposed [29]. The geometries and distribution of planar igneous bodies (i.e., sheet intrusions), such as dykes and sills, can determine emplacement mechanics, define melt source locations, and be used to reconstruct paleostress conditions [38].

The REPs investigated in this study show various intrusion shapes (sill, dyke, lenticular, zig-zag, brecciated, and irregular; see Table 2) which are distributed in the limestone as follows: (1) the western REP bodies show an ENE–WSW-trending linear alignment of lenticular bodies; (2) the main and submain REP bodies to an ENE–WSW-trending sub parallel alignment of lenticular bodies; and (3) the eastern REP bodies are dominated by an ENE–WSW-trending subparallel alignment of lenticular bodies. Dykes emplaced in the competent host rocks, such as igneous rocks, tend to form planar bodies that remain laterally by outcrop distances greater than 1 km. In contrast, dykes that invade dykes that intrude less competent hosts, such as micaceous schists, are more commonly ellipsoidal or occur as isolated bodies “like beads on a string” [29]. Dyke segmentation is a common process controlled by stress orientation, the properties of the host rocks, and dyke intrusion into already segmented fractures [39].

The main factors influencing the geometry and distribution of the Boam REPs are as follows:

(1) Pre-existing fracture sets: There are two recognized mechanisms of dyke propagation (e.g., [40]). First, when magma pressure exceeds the confining pressure, propagation can occur via the formation of new fractures. Second, magma propagation can occur via pre-existing fractures. Although there is still some debate, both of these mechanisms highlight the importance of fractures in controlling intrusion. In this study, the N–S-striking fracture sets were interpreted as pre-existing fractures, before intrusion. Thus, the identification of these pre-existing fractures can help interpret the paleostress applied during magma propagation. We suggest that the N–S-striking fractures provided a conduit that moderated the propagation of pegmatite. However, the main orientation of the REP is ENE–WSW (dominant directions of bedding), indicating the preferred direction of magma flow. Additional analyses (e.g., regional fracture pattern analysis, restoration, etc.) are needed to verify these interpretations.

(2) Bed contacts: Discontinuities in the host rock, such as bedding, foliation, and contact boundaries, can also act as fluid conduits in a similar way to fractures, and, thus, can have an important control on intrusion. According to Baer [41], differences in stress intensity between adjacent layers, interfaces with low shear resistance, and differences in shear moduli have significant effects on dyke propagation. Our study area comprises well-stratified limestone, which is in contact with the Yulri Series and the Dongsugok Formation, with alternating mudstone and sandstone thin layers. Although data on rock properties remain lacking, these rock types no doubt influenced the propagation of the REPs in the study region. Further work is required on rock properties to clarify these relationships. In addition, an examination of the geometry of the REPs that developed in

the Yulri and Wonnam Formations could help establish an exploration strategy for each rock type.

(3) Strain: The inferred dilation direction of the Boam REP is NNW–SSE based on the preferred orientation of the ENE–WSW-striking intrusions. The WNW–ESE-striking fault zone is interpreted as a post post-intrusive deformation feature. Although there is no direct evidence of horizontal movement, the NNE–SSW- and NE–SW-trending extension is associated with the vertical movement of the fault (northern block down). Therefore, the inferred deformation histories of the study area are as follows: Stage I = the development of the N–S-striking fracture set; Stage II = REP intrusion; and Stage III = displacement by the WNW–ESE-striking fault. Given that our interpretations are based on a two-dimensional study of the geometry and distribution of the REPs in this region, a subsequent three-dimensional analysis could usefully clarify our interpretations.

Overall, we have analyzed the intrusion patterns of REP and applied these to early-stage mineral exploration. However, the integration of structural data into a temperature model of the study area is essential to comprehensively understand REP forming systems in the study area [42–44].

## 6. Conclusions

(1) We mapped and provided detailed descriptions of the rare-element pegmatites of the Boam deposit in Uljin, South Korea, to inform mineral extraction. The rare-element pegmatites were found to vary in mineral assemblages from west to east, displaying (1) an inner K-feldspar ± quartz zone and (2) an outer plagioclase-mica-quartz ± K-feldspar zone. Li minerals are restricted to the pegmatite bodies and show pegmatite textures with greisen stage minerals. The origin of this zoning and greisen minerals is considered to be related to the differentiation of the pegmatites.

(2) Thirteen rare-element pegmatites are distributed within the Boam Li deposit. Our geometrical analysis showed that bed contact, fracture, and post post-intrusive deformation characteristics are key controls on the pegmatite intrusions. Therefore, for rare-element pegmatite exploration in this area, it is important to trace the bedding features, including local folding, and to fully understand the relationship between the pegmatites and the surrounding fracture systems.

(3) Recently, studies on the factors controlling shallow intrusions and their mechanisms have been increasingly conducted. Our work provides an understanding of the factors controlling acidic dykes developing in limestone strata, which can help improve understanding of intrusion in layered rock.

**Author Contributions:** Conceptualization, S.-J.Y. and I.-H.O.; methodology, S.-J.Y. and I.-H.O.; software, S.-J.Y.; formal analysis, I.-H.O.; investigation, S.-J.Y., I.-H.O., C.-H.H. and J.-H.L.; writing—original draft preparation, I.-H.O. and S.-J.Y.; writing—review and editing, S.-J.Y., I.-H.O. and E.-J.K.; funding acquisition, S.-J.C. All authors have read and agreed to the published version of the manuscript.

**Funding:** This research was supported by the Basic Research Project of the Korea Institute of Geoscience and Mineral Resources, Daejeon, South Korea, and funded by the Ministry of Science and ICT of Korea (GP2022-008).

**Data Availability Statement:** All data are shown in the tables of the article.

**Acknowledgments:** We appreciate the anonymous reviewers and the Associate Editor for their constructive review comments that improved the quality of the manuscript.

**Conflicts of Interest:** The authors declare no conflict of interest.

## References

1. Christmann, P.; Gloaguen, E.; Labbé, J.-F.; Melleton, J.; Piantone, P. Global lithium resources and sustainability issues. In *Lithium Process Chemistry*; Chagnes, A., Swiatowska, J., Eds.; Elsevier: Amsterdam, The Netherlands, 2015; pp. 1–40.
2. U.S. Geological Survey (USGS). *Mineral Commodity Summaries 2022: Lithium*; U.S. Geological Survey: Reston, VA, USA, 2022.

3. Kesler, S.E.; Gruber, P.W.; Medina, P.A.; Keoleian, G.A.; Everson, M.P.; Wallington, T.J. Global lithium resources: Relative importance of pegmatite, brine and other deposits. *Ore Geol. Rev.* **2012**, *48*, 55–69. [[CrossRef](#)]
4. Lee, B.H.; Koh, S.M.; Lee, G.J.; Jin, G.M.; Yang, S.J. *Preliminary Microscopic Mineralogical Study on Genetic Environment of Lithium Mica in Uljin Area*; Research Report JP2014–005–2015; Korea Institute of Geoscience and Mineral Resources: Daejeon, Korea, 2015; 68p.
5. Lee, G.J.; Kim, S.Y.; Koh, S.M. Potential evaluation of the Uljin lithium deposit. *Miner. Ind.* **2013**, *26*, 32–36.
6. Smith, L. Lithium Batteries—An Outlook and Summary. Available online: <https://www.coreconsultantsgroup.com/lithium-batteries-outlook-summary/> (accessed on 27 February 2022).
7. Wise, M.A.; Harmon, R.S.; Curry, A.; Jennings, M.; Grimac, Z.; Khashchevskaya, D. Handheld LIBS for Li exploration: An Example from the Carolina Tin-Spodumene Belt, USA. *Minerals* **2022**, *12*, 77. [[CrossRef](#)]
8. Linnen, R.L.; Van Lichtenvelde, M.; Černý, P. Granitic pegmatites as sources of strategic metals. *Elements* **2012**, *8*, 275–280. [[CrossRef](#)]
9. Li, J.K.; Liu, X.F.; Wang, D.H. The metallogenetic regularity of lithium deposit in China. *Acta Geol. Sin.* **2014**, *88*, 2269–2283.
10. Munk, L.A.; Boutt, D.F.; Hynek, S.A.; Moran, B.J. Hydrogeochemical fluxes and processes contributing to the formation of lithium-enriched brines in a hyper-arid continental basin. *Chem. Geol.* **2018**, *493*, 37–57. [[CrossRef](#)]
11. Goodenough, K.M.; Shaw, R.A.; Smith, M.; Estrade, G.; Marqu, E.; Bernard, C.; Nex, P. Economic mineralization in pegmatites: Comparing and contrasting NYF and LCT examples. *Can. Mineral.* **2019**, *57*, 753–755. [[CrossRef](#)]
12. Gao, Y.; Bagas, L.; Li, K.; Jin, M.; Liu, Y.; Teng, J. Newly discovered triassic lithium deposits in the Dahongliutan area, NorthWest China: A case study for the detection of lithium-bearing pegmatite deposits in rugged terrains using remote-sensing data and images. *Front. Earth Sci.* **2020**, *8*, 591966. [[CrossRef](#)]
13. Gourcerol, B.; Gloaguen, E.; Melleton, J.; Tuduri, J.; Galiegue, X. Re-assessing the European lithium resource potential—A review of hard-rock resources and metallogeny. *Ore Geol. Rev.* **2019**, *109*, 494–519. [[CrossRef](#)]
14. Cho, H.G. Li-bearing Tosudite from the Sungsan Mine, Korea. *J. Mineral. Soc. Korea* **1991**, *4*, 1–11.
15. Moon, S.H.; Park, H.I.; Ripley, E.M.; Lee, I. Mineralogic and stable isotope studies of Cassiterite Greisen mineralization in the Uljin Area, Korea. *Econ. Geol.* **1996**, *91*, 916–933. [[CrossRef](#)]
16. Lee, H.G.; Moon, H.S.; Oh, M.S. *Economic Mineral Deposits in Korea*, 1st ed.; Acanet: Seoul, Korea, 2007; 762p.
17. Kim, S.Y.; Seo, J.R.; Yang, J.I.; Kim, S.B. *Geology and Ore Deposits of Rare Elements in Hadong and Uljin Area, Korea*; Research Report KR-91-2D-1; Korea Institute of Geology, Mining & Materials: Daejeon, Korea, 1991; 156p.
18. Choi, Y.H.; Park, Y.R.; Noh, J.H. Genesis of Boam lithium deposits in Wangpiri, Uljin. *J. Geol. Soc. Korea* **2014**, *50*, 489–500. [[CrossRef](#)]
19. Selway, J.B.; Breaks, F.W.; Tindle, A.G. A review of rare-element (Li–Cs–Ta) pegmatite exploration techniques for the Superior Province, Canada, and large worldwide tantalum deposits. *Explor. Min. Geol.* **2006**, *14*, 1–30. [[CrossRef](#)]
20. Cheong, C.S.; Kil, Y.W.; Kim, J.; Jeong, Y.J.; Im, C.B. Geochemical characteristics of Precambrian basement rocks in the Jukbyeon area, northeastern Yeongnam massif, Korea. *J. Geol. Soc. Korea* **2004**, *40*, 481–499.
21. Lee, D.S.; Kang, J.H. Geological structures of the Hadong Northern Anorthosite Complex and its surrounding area in the Jirisan Province, Yeongnam Massif, Korea. *J. Pet. Soc. Korea* **2012**, *21*, 287–307.
22. Lee, D.W. Litho-geochemical Characteristics of Granitoids in Relation to Tin Mineralization in the Sangdong and Uljin Areas, Korea, and Their Application to Tin Exploration. Unpublished. Ph.D. Thesis, Seoul National University, Seoul, Korea, 1988; 153p.
23. Kim, N.H.; Cheong, C.S.; Park, K.H.; Kim, J.; Song, Y.S. Crustal evolution of northeastern Yeongnam Massif, Korea, revealed by SHRIMP U–Pb zircon geochronology and geochemistry. *Gondwana Res.* **2012**, *21*, 865–875. [[CrossRef](#)]
24. Cheong, A.C.S.; Jo, H.J. Tectonomagmatic evolution of a Jurassic Cordilleran flare-up along the Korean Peninsula: Geochronological and geochemical constraints from granitoid rocks. *Gondwana Res.* **2020**, *88*, 21–44. [[CrossRef](#)]
25. London, D. *Pegmatites*; The Canadian Mineralogist, Special Publication; The Mineralogical Association: Québec, QC, Canada, 2008; Volume 10, 340p.
26. Černý, P.; Blevin, P.L.; Cuney, M.; London, D. Granite-related ore deposits. In *Economic Geology: 100th Anniversary Volume*; Society of Economic Geologists: Littleton, CO, USA, 2005; pp. 337–370.
27. London, D. Geochemistry of alkali and alkaline earth elements in ore-forming granites, pegmatites and rhyolites. In *Rare Element Geochemistry and Mineral Deposits*; Linnen, R.L., Samson, I.M., Eds.; Geological Association of Canada: St. John's, NL, Canada, 2005; Volume 17, pp. 17–43.
28. Barros, R.; Kaeter, D.; Menuge, J.F.; Skoda, R. Controls on chemical evolution and rare element enrichment in crystallising albite-spodumene pegmatite and wallrocks: Constraints from mineral chemistry. *Lithos* **2020**, 352–353, 105289. [[CrossRef](#)]
29. London, D. Ore-forming processes within granitic pegmatites. *Ore Geol. Rev.* **2018**, *101*, 349–383. [[CrossRef](#)]
30. Huang, H.; Wang, T.; Zhang, Z.C.; Li, C.; Qin, Q. Highly differentiated fluorine-rich, alkaline granitic magma linked to rare metal mineralization: A case study from the Boziguo'er rare metal granitic pluton in South Tianshan Terrane, Xinjiang, NW China. *Ore Geol. Rev.* **2018**, *96*, 146–163. [[CrossRef](#)]
31. Wu, H.H.; Huang, H.; Zhang, Z.C.; Wang, T.; Guo, L.; Zhang, Y.H.; Wang, W. Geochronology, geochemistry, mineralogy and metallogenic implications of the Zhaojinggou Nb-Ta deposit in the northern margin of the North China Craton, China. *Ore Geol. Rev.* **2020**, *125*, 103692. [[CrossRef](#)]

32. Ballouard, C.; Elburg, M.A.; Tappe, S.; Reinke, C.; Ueckermann, H.; Doggart, S. Magmatic-hydrothermal evolution of rare metal pegmatites from the Mesoproterozoic Orange River pegmatite belt (Namaqualand, South Africa). *Ore Geol. Rev.* **2020**, *116*, 103252. [[CrossRef](#)]
33. Shearer, C.K.; Papike, J.J.; Simon, S.B. Pegmatite-wallrock interactions, Black Hills, South Dakota: Interaction between pegmatite-derived fluids and quartz-mica schist wallrock. *Am. Mineral.* **1986**, *71*, 518–539.
34. Dittrich, T.; Seifert, T.; Schulz, B.; Hagemann, S.; Gerdes, A.; Pfänder, J. *Archean Rare-Metal Pegmatites in Zimbabwe and Western Australia: Geology and Metallogeny of Pollucite Mineralisations*, 1st ed.; Springer: Heidelberg, Germany, 2019; 125p.
35. KIGAM. *Development of Precise Exploration Technology for Energy Storage Minerals (V) Existing in Korea and the Resources Estimation*; Research Report GP2020–007–2021; Korea Institute of Geoscience and Mineral Resources: Daejeon, Korea, 2021; 216p.
36. Bradley, D.C.; McCauley, A.D.; Stillings, L.M. *Mineral-Deposit Model for Lithium-Cesium-Tantalum Pegmatites*; Scientific Investigations Report 2010–5070–O; U.S. Geological Survey: Reston, VA, USA, 2017; 32p.
37. Pirajno, F. *Hydrothermal Mineral Deposit*; Springer: Berlin/Heidelberg, Germany, 1992; pp. 101–155.
38. Magee, C.; Muirhead, J.; Schofield, N.; Walker, R.; Galland, O.; Holford, S.; Spacapan, J.; Jackson, C.; McCarthy, W. Structural signatures of igneous sheet intrusion propagation. *J. Struct. Geol.* **2019**, *125*, 148–154. [[CrossRef](#)]
39. Baer, G.; Beyth, M. A mechanism of dyke segmentation in fractured host rock. In *Mafic Dykes and Emplacement Mechanisms*; Parker, A.J., Rickwood, P.C., Tucker, D.H., Eds.; A.A. Balkema: Rotterdam, The Netherlands, 1990; pp. 3–11.
40. Yang, S.J.; Kim, Y.S. Descriptive classification of dyke morphologies based on similarity to fracture geometries. *Geosci. J.* **2022**, *26*, 79–93. [[CrossRef](#)]
41. Baer, G. Mechanisms of Dike Propagation in Layered Rocks and in Massive, Porous Sedimentary Rocks. *J. Geophys. Res.* **1991**, *96*, 11911–11929. [[CrossRef](#)]
42. Dill, H.G. The CMS classification scheme (Chemical composition—Mineral assemblage—Structural geology)—Linking geology to mineralogy of pegmatitic and aplitic rocks. *Neues Jahrb. Mineral. Abh.* **2016**, *193*, 231–263. [[CrossRef](#)]
43. Dill, H.G. Geology and chemistry of Variscan-type pegmatite systems (SE Germany)—With special reference to structural and chemical pattern recognition of felsic mobile components in the crust. *Ore Geol. Rev.* **2018**, *92*, 205–239. [[CrossRef](#)]
44. Ronchi, F.C.; Althoff, F.J.; Bastos Neto, A.C.; Dill, H.G. Structural control of REE-pegmatites associated with the world class Sn-Nb-Ta-cryolite deposit at the Pitinga mine, Amazonas, Brazil. *Pesqui. Geociênc.* **2019**, *46*, e0734.